Evidence for charge transfer and proximate magnetism in graphene-α-RuCl₃ heterostructures

Boyi Zhou and J. Balgley

Department of Physics, Washington University in St. Louis, 1 Brookings Drive, St. Louis, Missouri 63130, USA

P. Lampen-Kelley, J.-Q. Yan, and D. G. Mandrus

Material Science & Technology Division, Oak Ridge National Laboratory, Oak Ridge, Tennessee 37831, USA and Department of Material Science and Engineering, University of Tennessee, Knoxville, Tennessee 37996, USA

E. A. Henriksen •*

Department of Physics, Washington University in St. Louis, 1 Brookings Drive, St. Louis, Missouri 63130, USA and Institute for Materials Science & Engineering, Washington University in St. Louis, 1 Brookings Drive, St. Louis, Missouri 63130, USA



(Received 24 July 2019; published 28 October 2019)

We report a study of electronic transport in van der Waals heterostructures composed of flakes of the antiferromagnetic Mott insulator α -RuCl₃ placed on top of monolayer graphene Hall bars. While the zero-field transport shows a strong resemblance to that of isolated graphene, we find a consistently p-type Hall effect suggestive of multiband conduction, along with a nonmonotonic and gate-voltage-dependent excursion of the resistivity at low temperatures that is reminiscent of transport in the presence of a magnetic phase transition. We interpret these data as evidence for charge transfer from graphene to α -RuCl₃ in an inhomogeneous device yielding both highly and lightly doped regions of graphene, while the latter shows a particular sensitivity to magnetism in the α -RuCl₃. Thus proximity to graphene is a means to access magnetic properties of thin layers of magnetic insulators.

DOI: 10.1103/PhysRevB.100.165426

I. INTRODUCTION

The layered Mott insulator α -RuCl₃ exhibits phenomena consistent with quantum spin-liquid behavior [1–8]. Particularly intriguing among recent discoveries is a half-integer quantized thermal Hall conductance [9], which may signal the presence of non-Abelian excitations useful in creating a topological quantum bit [10]. Recent studies of α -RuCl₃ employ a variety of bulk magnetic probes on high quality samples, mm to cm scale in size, which are generally found to behave as Kitaev paramagnets at temperatures above $T_{\text{N\'eel}}$ of a zigzag antiferromagnet [2,4–8]. Despite the convenience of electronic transport, it is not widely used due to the Mott insulating nature of α -RuCl₃ [11–15].

Seeking to probe α-RuCl₃ by electronic methods, we have studied the electronic transport in heterostructures comprised of α-RuCl₃ stacked on monolayer graphene. Incorporating graphene into stacks of various layered materials or thin films is a promising approach to discover new physics and potential applications [16]. In particular, graphene layered with various magnetic insulators including YIG, EuO, and EuS has been proposed as a platform for new magnetic phases or proximity-induced magnetism [17–22]. Proximity effects for graphene in contact with the antiferromagnets BiFeO₃ and RbMnCl₃ have also been theoretically considered [23,24], though in both cases the graphene interacts with ferromagnetically aligned spins. Meanwhile, the precise nature of the

interface of graphene with other materials is of much current interest, for instance in graphene layered with transition metal dichalcogenides where a charge-transfer or even spin-orbit-proximity effect has been found [25–28].

Here we explore transport in graphene next to an antiferromagnetic Mott insulator with the potential for quantum spin-liquid physics [2–9]. We find the transport in these devices—which at first glance is very similar to that of standard graphene-on-SiO₂—nonetheless shows a strongly enhanced conductivity and clear signatures of multiband transport. While the presence of a Dirac peak associated with graphene would appear to suggest that no charge transfer has occurred despite the different work functions of graphene and α -RuCl₃, the Hall effect shows robust evidence for a sizable population of holes in coexistence with the standard graphene gate-voltage-dependent transport. Moreover between 15 and 40 K, we find a nonmonotonic temperature dependence of the resistivity, suggestive of transport in the presence of magnetic phase transitions. While α -RuCl₃ has a $T_{\text{N\'eel}}$ of 7 or 14 K depending on structural disorder [29], here the implied critical temperatures are roughly twice as large. Altogether, our data are consistent with a picture of inhomogeneous transport where the graphene and α -RuCl₃ are intermittently in contact yielding regions that are either lightly or highly doped, the latter arising from an expected charge transfer between graphene and α -RuCl₃ [30] that is also predicted to reinforce the antiferromagnetism. Finally, the gate-voltage dependence of the magnetic signatures suggests it occurs in the lightly doped regions that in our picture are not in direct contact with the α -RuCl₃.

^{*}henriksen@wustl.edu

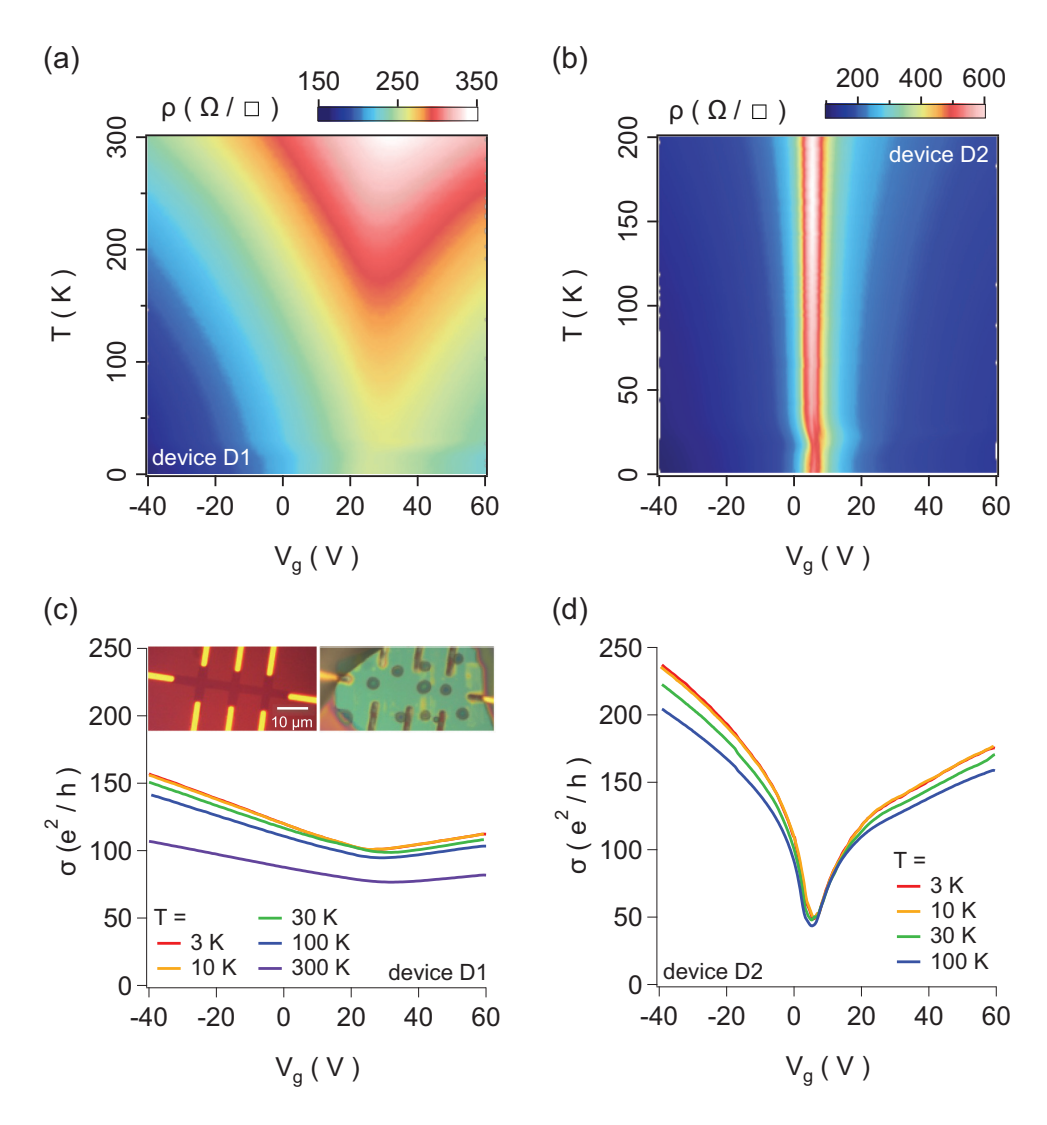


FIG. 1. Transport at zero magnetic field. Though similar in appearance to the usual electronic transport in graphene-on-oxide, the minimum conductivity is much larger than expected. (a),(b) Resistivity vs temperature and gate voltage in two representative devices, D1 and D2, respectively. (c),(d) Constant-temperature line cuts of (a) and (b), replotted as the conductivity, $\sigma = 1/\rho$. Inset to (c) are images of device D1 showing the monolayer graphene Hall bar before (left) and after (right) being covered by a \sim 10-nm-thick α -RuCl₃ flake. Circular features are remnant spots from a polycarbonate layer used in transferring the flake.

II. EXPERIMENT

Single crystals of α -RuCl₃ were grown using a vapor transport technique from phase pure commercial α -RuCl₃ powder [7]. The devices consist of monolayer graphene exfoliated on Si wafers with a 300-nm-thick surface oxide layer. The graphene is etched into a Hall bar pattern using a patterned polymethyl-methacrylate mask and an O_2 plasma, followed by standard thin-film patterning for contacts made of 3/30 nm of Cr/Au. The graphene surface is then cleaned by sweeping with an atomic force microscope tip in contact mode, which serves to remove the remnant nm-thick layer of electron beam resist [14,31–34]. A flake of α -RuCl₃, exfoliated from parent crystals onto separate oxidized wafers [35], is then transferred on top of the graphene using a polycarbonate film stretched over a small silicone stamp. The α -RuCl₃ flakes range in thickness from 5 to 25 nm (\sim 10–40 layers) thick; prior Raman spectroscopy of flakes of comparable thickness give the same spectra as a pristine bulk sample [35]. Images of a typical device are shown inset to Fig. 1(c) before and after transferring the α -RuCl₃ flake. All measurements were performed using standard low-frequency lock-in techniques in a variable temperature cryostat with a 9-T magnet, using gate voltages applied to the Si substrates. The graphene carrier density was determined either directly from analysis of Shubnikov–de Haas oscillations, or by known calibrations for the wafers used in these devices [36], $n = 7.2 \times 10^{10} \times (V_g - V_{\rm DP}) \ {\rm cm^{-2} \, V^{-1}}$, where $V_{\rm DP}$ is the voltage at which the Dirac peak is observed.

III. RESULTS

A. Zero-field transport

The four-terminal resistivity at zero magnetic field of two representative devices is shown in Figs. 1(a) and 1(b) vs both the back gate voltage V_g and temperature T. These data are clearly akin to typical graphene-on-oxide transport:

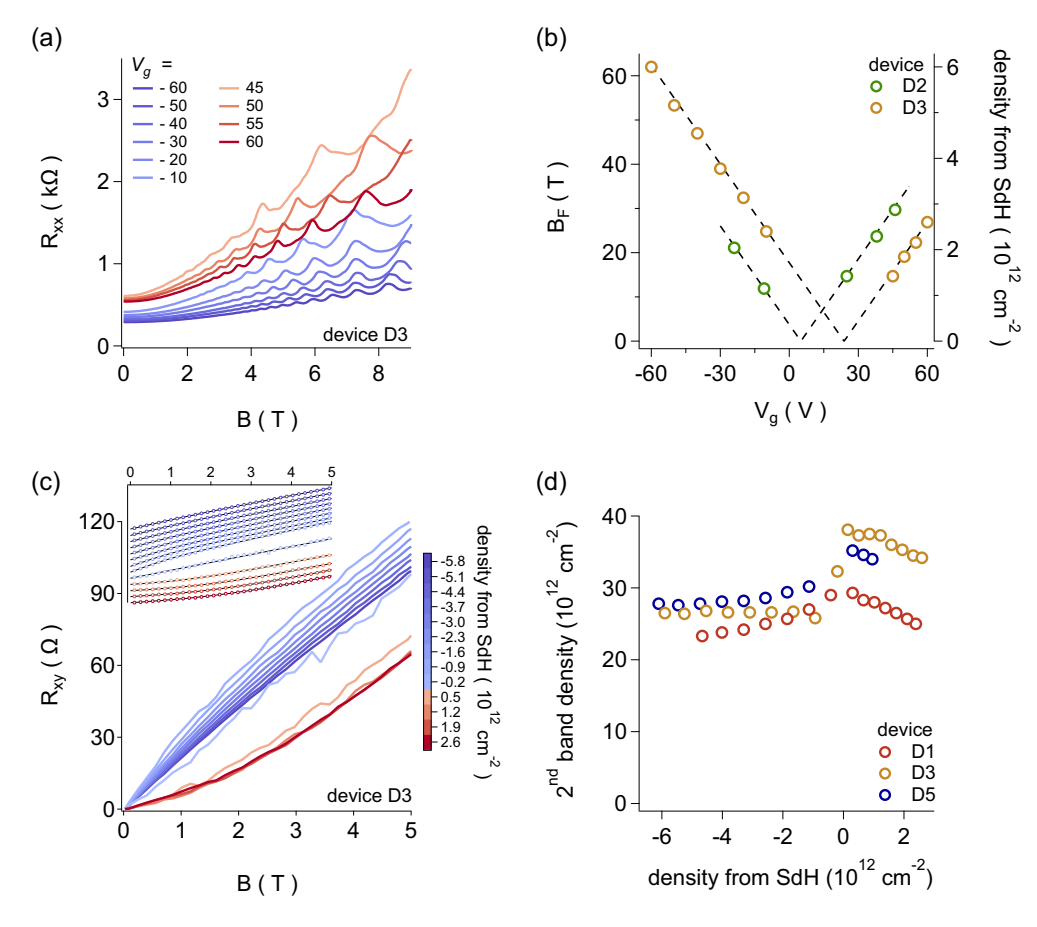


FIG. 2. Magnetotransport of graphene– α -RuCl₃ devices. (a) Shubnikov–de Haas oscillations from device D3 for a range of gate voltages on either side of the minimum conductivity (here at $V_g = 25$ V). (b) The SdH oscillation frequency B_F for two devices. The corresponding charge density $n = gB_f/\phi_0$ (where we assume g = 4 degrees of freedom as for graphene and ϕ_0 is the magnetic-flux quantum) is marked on the right axis. Dashed lines show the expected graphene density, $n = \alpha(V_g - V_{DP})$, based on prior measurements of isolated graphene flakes on the same substrates, with $\alpha = 7.2 \times 10^{10}$ carriers/cm²/V and V_{DP} is the location of the zero-field conductivity minimum. (c) Main panel: Hall resistance for D3 acquired over a range of gate voltages [converted to carrier densities by the calibration in (b)]. The colors correspond to those in (a), and include three additional traces at densities close to charge neutrality that did not exhibit SdH oscillations. Inset: the same data, vertically offset for clarity, with fits (black lines) to a two-band model of magnetotransport. (d) Carrier densities of the second band determined from two-band model fits.

a maximum in the resistivity ("Dirac peak") appears as V_g is swept, which is rather broad in Fig. 1(a) and narrower in Fig. 1(b). All devices explored show similar behavior [14], with a range of Dirac peak widths and gate voltage locations of the peak ($V_{\rm DP}$). A decrease in the resistivity with temperature is seen that is consistent with a reduction in phonon scattering [37].

A marked departure from standard graphene transport becomes clear in Figs. 1(c) and 1(d) where we show constant temperature profiles from Figs. 1(a) and 1(b), respectively, replotted as the conductivity σ . For all traces, σ increases monotonically with increasing gate voltage to either side of the local conductivity minimum σ_{\min} , which in isolated graphene marks the charge neutrality point (here σ_{\min} occurs at $V_{\rm DP} = +23$ V and +5 V for D1 and D2, respectively). However, the values of σ_{\min} in *every* device are anomalously large, with values as high as 50 or 100 e^2 /h at T=3 K; the highest we have found so far is 240 e^2 /h. This stands in sharp contrast to the typical $\sigma_{\min} = 2 - 12 e^2$ /h routinely observed in regular graphene-on-oxide devices [38–40]. To

directly verify this conductivity enhancement, we fabricated a long Hall bar and transferred flakes of α -RuCl₃ on one half and hexagonal boron nitride on the other, and found the resistivity of the α -RuCl₃ -covered region to be an order of magnitude lower than the boron nitride covered portion [14].

B. Low-field transport

Shubnikov–de Haas oscillations can be discerned in the magnetoresistance of some devices, as shown in Fig. 2(a) for a range of gate voltages on either side of the conductivity minimum for device D3. In Fig. 2(b) we plot the frequency B_F of the oscillations in 1/B as a function of V_g for devices D2 and D3, and calculate the corresponding density of charge carriers participating in the SdH oscillations from $B_F = n\phi_0/g$ assuming g = 4 which counts the usual spin and valley degeneracies in graphene, and $\phi_0 = h/e$ is the magnetic flux quantum. The densities derived in this way correlate precisely with prior calibrations of the charge-gating efficiency of our Si/SiO₂ substrates. In other words, the SdH oscillations reveal

bipolar behavior and a charge neutrality point, consistent with the usual graphene picture but for the enhanced conductivity which, in this device, appears as a minimum conductivity at $T=2~{\rm K}$ of 63 $e^2/{\rm h}$.

In contrast, the Hall resistance R_{xy} shown in Fig. 2(c) is markedly different from typical graphene behavior. In particular, (i) R_{xy} is nonlinear, with (ii) values well below the Hall resistance of isolated graphene at equivalent charge densities, and (iii) surprisingly, as the graphene charge density is gated from p to n type, the Hall resistance does not change sign; indeed, the sign remains consistent with overall p-type transport. Since altogether we observe graphenelike behavior albeit with a higher conductivity and unusual Hall response, we analyze the data in a two-band model of graphene transport plus a second conducting band whose origin we will discuss later. In the inset to Fig. 2(c) we replot the Hall data with the traces offset for clarity, and perform curve fits using the standard two-band formalism [41],

$$R_{xy} = \frac{B}{e} \frac{n_1 \mu_1^2 + n_2 \mu_2^2 + (n_1 + n_2)(\mu_1 \mu_2 B)^2}{(|n_1|\mu_1 + |n_2|\mu_2)^2 + (n_1 + n_2)^2(\mu_1 \mu_2 B)^2}, \quad (1)$$

where n_i and μ_i are the density and mobility of the ith band. For n_1 we use the graphene densities calibrated either from SdH oscillations or use the known gating efficiency for graphene-on-oxide; see Fig. 2. We also require the fitting coefficients to reproduce the zero-field conductivity, $\sigma_0 =$ $e(n_1\mu_1 + n_2\mu_2)$. The resulting charge density of the second band, determined from measurements in three devices, is plotted in Fig. 2(d) vs the SdH-derived density. The sign of n_2 is holelike, the magnitude is roughly an order of magnitude larger than the densities in the graphene, and there is a weak dependence on the density of the graphene band with either a step or peak at the charge neutrality point. The good fit to the Hall data and the consistent results among different samples are strong evidence for the presence of a second conducting band. Plots of the mobilities extracted for each band are included in the Supplemental Material [14]. The graphene band mobilities are typically 2000-6000 cm²/V s, reasonable for graphene-on-oxide devices; the mobilities of the second band lie between 500 and 2000 cm^2/V s.

C. Temperature-dependent transport

Returning to Figs. 1(a) and 1(b), an additional feature is visible around 20 K that is not normally present in graphene. We highlight this by plotting the normalized temperature derivative of the resistivity for devices D1 and D2 in Figs. 3(a)-3(c) and 3(d)-3(f), respectively (corresponding line cuts of the resistivity itself are included in the Supplemental Material [14]). Intriguing line shapes appear with peaks and dips whose specific shapes are distinctly different for por *n*-type graphene, and for which the peak temperatures show a sharp drop right at charge neutrality. We tentatively attribute this behavior to the presence of magnetic phase transitions. Bulk α-RuCl₃ is a zigzag antiferromagnet with $T_{\text{N\'eel}} = 7$ or 14 K depending on the stacking order [29]. It is well known that the electrical resistivity can be impacted by magnetic transitions [42,43], with the shape of $d\rho/dT$ in the neighborhood of a magnetic transition being generically linked to the nature of the magnetism, e.g., a peak is often

associated with ferromagnetism where T_{Curie} is at the peak maximum, and a peak/dip structure is expected for antiferromagnets with $T_{\text{N\'eel}}$ at the dip minimum [44–46]. By analogy to this prior literature we suggest that a magnetic phase transition occurs in, or near, the graphene– α -RuCl₃ interface, and that the nature of this transition depends on the charge state of the graphene. While concrete identification of distinct phases is preliminary, the shape of $d\rho/dT$ is clearly correlated with the graphene charge-carrier density and the visible Dirac peak; we include data for additional samples in the Supplemental Material [14]. The transition temperatures implied by the peak and dip locations in Fig. 3 lie in the range of 12–35 K, rather higher than the 7- or 14-K antiferromagnetic transition in bulk α -RuCl₃ [29].

IV. DISCUSSION

In sum, in heterostructures of graphene next to α -RuCl₃ we observe a conductivity enhancement over that of isolated graphene, p-type Hall effect, and signatures of magnetic transitions. The differing work functions of graphene, at 4.6 eV [47], and α -RuCl₃, at 6.1 eV [48], strongly imply a transfer of electrons from graphene to α -RuCl₃ will take place when the two materials come in contact, and indeed recent ab initio calculations predict a charge transfer from monolayer graphene to monolayer α -RuCl₃ at the level of 4.7% of an electron per Ru atom, along with a concomitant change in the magnetic couplings in α -RuCl₃ [30]. However in the graphene– α -RuCl₃ heterostructure, (1) the gate voltage location of the Dirac peak—which is highly sensitive to extrinsic charge doping [36,40]—is well within the usual range for grapheneon-oxide devices, suggesting no significant charge transfer from graphene has taken place, yet (2) the Hall effect shows clear evidence for two-band transport with population of holes well in excess of what is expected for the small shift of the Dirac peak away from $V_g = 0$. We resolve this by proposing the coexistence of both lightly and highly doped regions of the graphene, due to the graphene and α -RuCl₃ flake not being in uniform contact. Wherever the two sheets are in close contact, the charge transfer expected from the work function difference occurs, but wherever they are separated the graphene remains nominally undoped. Indeed vdW devices often exhibit bubbles between the layers, and it is plausible the oxidesupported graphene inherits a nm-scale roughness so only higher-lying parts make contact with the overlying α -RuCl₃ flake. Thus transport measurements can yield a clear Dirac peak due to the intrinsic graphene, in parallel with highly hole-doped graphene with a second charge neutrality point well outside the accessible V_g range. In principle, since the α -RuCl₃ will have gained the balancing charge density, it may become conducting as well though this is not resolved here. We note that given the factor of 6 difference in areal density of C atoms in graphene to Ru atoms in α -RuCl₃, the predicted charge transfer [30] corresponds to a loss of roughly 0.8% electrons/C from the graphene, or 2.8×10^{13} cm⁻², which is remarkably close to the density of holes found in the second band in the nonlinear Hall analysis. Recently this charge transfer has been observed in graphene–α-RuCl₃ devices fabricated on boron nitride, but without the attendant magnetic signatures [49].

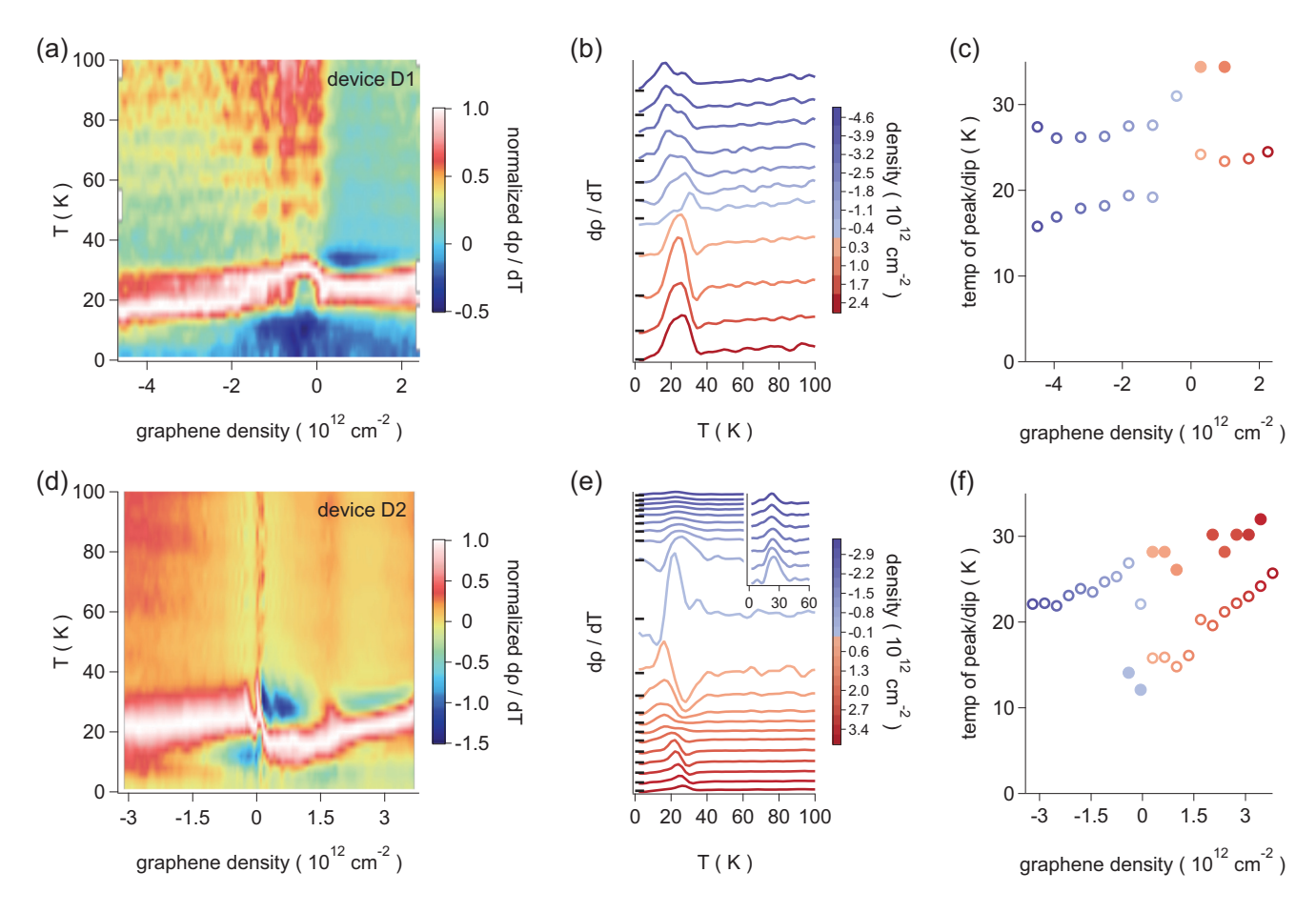


FIG. 3. Transport signatures of magnetic transitions. The resistivity of graphene– α -RuCl₃ heterostructures shows characteristics of magnetic transitions [42–46]. These data are for the same two devices as in Fig. 1: D1 (a)–(c) and D2 (d)–(f). (a),(d) Color maps showing $d\rho/dT$ vs the graphene charge-carrier density in each device, normalized by the maximum value of $d\rho/dT$ below 60 K at each density. This highlights the evolution in temperature at which peaks in $d\rho/dT$ are observed to occur. (b)–(e) Line cuts of $d\rho/dT$ from (a) and (d), offset vertically and not normalized in order to show the variation in amplitude of the peaks and dips. Blue-to-red shading follows the transition from p- to n-type doping of the graphene, with charge neutrality at the blue/red border. The inset to (e) shows a $12\times$ magnified view of the top p-type traces. Short black lines along the left axis mark the location of $d\rho/dT=0$ for each trace. (c),(f) Temperatures of the $d\rho/dT$ peak maxima (open circles) and dip minima (filled circles). For D1 (a)–(c) two peaks can be discerned for p-type graphene. In both devices, the peak temperatures show a sharp variation at charge neutrality in graphene.

The V_g dependence of $d\rho/dT$ generically reflects the presence of the charge neutrality point in graphene. This suggests the magnetic response is arising from the lightly doped graphene regions that lie very close to but do not contact the α -RuCl₃ flake. We cannot rule out a magnetic response from the highly doped regions as well, but expect the lightly doped regions should be more sensitive to large fluctuations of the spin correlations in α -RuCl₃ near a magnetic transition. Thus the inhomogeneous nature of the samples fortuitously provides a window on magnetic effects arising at or near the interface. We note the elevated magnetic transition temperatures inferred above are consistent with an enhancement of magnetic couplings expected from the graphene– α -RuCl₃ charge transfer [30].

We conclude with some general observations: (1) The Mott insulating nature of α -RuCl₃ may play a role here. The band gap of strongly correlated materials prepared as thin films on metals can be reduced over the bulk value due to screening of the Coulomb interaction, as observed

for C_{60} on silver [50]. While the density of states in a thick silver film certainly is more effective at screening than a monolayer of graphene, there is still the question of how added $\sim 3 \times 10^{13}$ -cm⁻² electrons in α -RuCl₃ will impact its electronic structure. (2) No dependence on the α -RuCl₃ flake thickness has been seen. Since the α -RuCl₃ layers are weakly bound together, it may be that only the one or two α -RuCl₃ layers closest to graphene are impacted by proximity. This could amplify the already considerable magnetic anisotropy [51,52], and so account for the enhanced magnetic transition temperatures we observe. (3) The detailed transport behavior is certain to depend on the nature of the graphene–α-RuCl₃ interface, in particular by the presence of remnant disorder (e.g., water and incidental adsorbates accrued during fabrication) or the possibility of surface reconstruction effects [53]. Notably, the Ru atoms are arranged in a honeycomb lattice as for C in graphene, with the two lattices close to a 2:5 commensurability so that moiré physics may not be irrelevant [54].

V. CONCLUSION

We have studied the electronic transport in monolayer graphene devices with a proximate α -RuCl₃ flake. The transport shows signatures of undoped graphene conducting in parallel to a large population of holes. We interpret this as transport at an inhomogeneous interface composed of both lightly and highly doped graphene, the latter arising from a significant charge transfer of electrons from graphene to α -RuCl₃. The resistivity at low temperatures shows signs of a magnetic phase transition that we interpret as a proximity effect appearing in the transport through the lightly doped graphene regions.

ACKNOWLEDGMENTS

We wish to thank A. Banerjee, S. Biswas, E. Gerber, E.-A. Kim, A. MacDonald, S. Nagler, R. Valenti, and J. van den Brink for informative discussions. We acknowledge support from the Institute of Materials Science and Engineering at Washington University in St. Louis. E.A.H., B.Z., and J.B. acknowledge support under Grant No. NSF DMR-1810305. D.G.M. and P.L.-K. acknowledge support from the Gordon and Betty Moore Foundation EPiQS Initiative through Grant No. GBMF4416.

- [1] A. Y. Kitaev, Anyons in an exactly solved model and beyond, Ann. Phys. **321**, 2 (2006).
- [2] L. J. Sandilands, Y. Tian, K. W. Plumb, Y.-J. Kim, and K. S. Burch, Scattering Continuum and Possible Fractionalized Excitations in α-RuCl₃, Phys. Rev. Lett. **114**, 147201 (2015).
- [3] A. Banerjee, C. A. Bridges, J. Q. Yan, A. A. Aczel, L. Li, M. B. Stone, G. E. Granroth, M. D. Lumsden, Y. Yiu, J. Knolle, S. Bhattacharjee, D. L. Kovrizhin, R. Moessner, D. A. Tennant, D. G. Mandrus, and S. E. Nagler, Proximate Kitaev quantum spin liquid behavior in a honeycomb magnet, Nat. Mater. 15, 733 (2016).
- [4] S. H. Baek, S. H. Do, K. Y. Choi, Y. S. Kwon, A. U. B. Wolter, S. Nishimoto, J. van den Brink, and B. Büchner, Evidence for a Field-Induced Quantum Spin Liquid in α-RuCl₃, Phys. Rev. Lett. 119, 037201 (2017).
- [5] S.-H. Do, S.-Y. Park, J. Yoshitake, J. Nasu, Y. Motome, Y. Kwon, D. T. Adroja, D. J. Voneshen, K. Kim, T.-H. Jang, J.-H. Park, K.-Y. Choi, and S. Ji, Majorana fermions in the Kitaev quantum spin system α-RuCl₃, Nat. Phys. 13, 1079 (2017).
- [6] J. Zheng, K. Ran, T. Li, J. Wang, P. Wang, B. Liu, Z.-X. Liu, B. Normand, J. Wen, and W. Yu, Gapless Spin Excitations in the Field-Induced Quantum Spin Liquid Phase of α-RuCl₃, Phys. Rev. Lett. 119, 227208 (2017).
- [7] A. Banerjee, J. Yan, J. Knolle, C. A. Bridges, M. B. Stone, M. D. Lumsden, D. G. Mandrus, D. A. Tennant, R. Moessner, and S. E. Nagler, Neutron scattering in the proximate quantum spin liquid α-RuCl₃, Science 356, 1055 (2017).
- [8] N. Janša, A. Zorko, M. Gomilšek, M. Pregelj, K. W. Krämer, D. Biner, A. Biffin, C. Rüegg, and M. Klanjšek, Observation of two types of fractional excitation in the Kitaev honeycomb magnet, Nat. Phys. 14, 786 (2018).
- [9] Y. Kasahara, T. Ohnishi, Y. Mizukami, O. Tanaka, S. Ma, K. Sugii, N. Kurita, H. Tanaka, J. Nasu, Y. Motome, T. Shibauchi, and Y. Matsuda, Majorana quantization and half-integer thermal quantum Hall effect in a Kitaev spin liquid, Nature (London) 559, 227 (2018).
- [10] A. Y. Kitaev, Fault-tolerant quantum computation by anyons, Ann. Phys. **303**, 2 (2003).
- [11] L. Binotto, I. Pollini, and G. Spinolo, Optical and transport properties of the magnetic semiconductor α-RuCl₃, Phys. Status Solidi B **44**, 245 (1971).
- [12] S. Rojas and G. Spinolo, Hall effect in α -RuCl₃, Solid State Commun. **48**, 349 (1983).

- [13] S. Mashhadi, D. Weber, L. M. Schoop, A. Schulz, B. V. Lotsch, M. Burghard, and K. Kern, Electrical transport signature of the magnetic fluctuation-structure relation in α-RuCl₃ nanoflakes, Nano Lett. 18, 3203 (2018).
- [14] See Supplemental Material at http://link.aps.org/supplemental/ 10.1103/PhysRevB.100.165426 which includes further information on sample details, measurements of transport in additional samples, and discussion of the transport models.
- [15] K. W. Plumb, J. P. Clancy, L. J. Sandilands, V. V. Shankar, Y. F. Hu, K. S. Burch, H.-Y. Kee, and Y.-J. Kim, α-RuCl₃: A spin-orbit assisted Mott insulator on a honeycomb lattice, Phys. Rev. B 90, 041112(R) (2014).
- [16] A. K. Geim and I. V. Grigorieva, Van der Waals heterostructures, Nature (London) 499, 419 (2013).
- [17] H. Haugen, D. Huertas-Hernando, and A. Brataas, Spin transport in proximity-induced ferromagnetic graphene, Phys. Rev. B 77, 115406 (2008).
- [18] H. X. Yang, A. Hallal, D. Terrade, X. Waintal, S. Roche, and M. Chshiev, Proximity Effects Induced in Graphene by Magnetic Insulators: First-Principles Calculations on Spin Filtering and Exchange-Splitting Gaps, Phys. Rev. Lett. 110, 046603 (2013).
- [19] J. Zhang, C. Triola, and E. Rossi, Proximity Effect in Graphene-Topological-Insulator Heterostructures, Phys. Rev. Lett. 112, 096802 (2014).
- [20] Z. Wang, C. Tang, R. Sachs, Y. Barlas, and J. Shi, Proximity-Induced Ferromagnetism in Graphene Revealed by the Anomalous Hall Effect, Phys. Rev. Lett. 114, 016603 (2015).
- [21] P. Wei, S. Lee, F. Lemaitre, L. Pinel, D. Cutaia, W. Cha, F. Katmis, Y. Zhu, D. Heiman, J. Hone, J. S. Moodera, and C.-T. Chen, Strong interfacial exchange field in the graphene/EuS heterostructure, Nat. Mater. 15, 711 (2016).
- [22] S. Su, Y. Barlas, J. Li, J. Shi, and R. K. Lake, Effect of intervalley interaction on band topology of commensurate graphene/EuO heterostructures, Phys. Rev. B 95, 075418 (2017).
- [23] Z. Qiao, W. Ren, H. Chen, L. Bellaiche, Z. Zhang, A. H. MacDonald, and Q. Niu, Quantum Anomalous Hall Effect in Graphene Proximity Coupled to an Antiferromagnetic Insulator, Phys. Rev. Lett. 112, 116404 (2014).
- [24] J. Zhang, B. Zhao, Y. Yao, and Z. Yang, Quantum anomalous Hall effect in graphene-based heterostructure, Sci. Rep. 5, 10629 (2015).

- [25] J. He, N. Kumar, M. Z. Bellus, H.-Y. Chiu, D. He, Y. Wang, and H. Zhao, Electron transfer and coupling in graphene-tungsten disulfide van der Waals heterostructures, Nat. Commun. 5, 5622 (2014).
- [26] L. Yuan, T.-F. Chung, A. Kuc, Y. Wan, Y. Xu, Y. P. Chen, T. Heine, and L. Huang, Photocarrier generation from interlayer charge-transfer transitions in WS₂-graphene heterostructures, Sci. Adv. 4, e1700324 (2018).
- [27] W. Lin, P. Zhuang, H. Chou, Y. Gu, R. Roberts, W. Li, S. K. Banerjee, W. Cai, and D. Akinwande, Electron redistribution and energy transfer in graphene/MoS₂ heterostructure, Appl. Phys. Lett. 114, 113103 (2019).
- [28] J. O. Island, X. Cui, C. Lewandowski, J. Y. Khoo, E. M. Spanton, H. Zhou, D. Rhodes, J. C. Hone, T. Taniguchi, K. Watanabe, L. S. Levitov, M. P. Zaletel, and A. F. Young, Spin-orbit-driven band inversion in bilayer graphene by the van der Waals proximity effect, Nature 571, 85 (2019).
- [29] H. B. Cao, A. Banerjee, J.-Q. Yan, C. A. Bridges, M. D. Lumsden, D. G. Mandrus, D. A. Tennant, B. C. Chakoumakos, and S. E. Nagler, Low-temperature crystal and magnetic structure of α-RuCl₃, Phys. Rev. B **93**, 134423 (2016).
- [30] E. Gerber, Y. Yao, T. A. Arias, and E.-A. Kim, Ab initio mismatched interface theory of graphene on α-RuCl₃: Doping and magnetism, arXiv:1902.09550.
- [31] A. M. Goossens, V. E. Calado, A. Barreiro, K. Watanabe, T. Taniguchi, and L. M. K. Vandersypen, Mechanical cleaning of graphene, Appl. Phys. Lett. 100, 073110 (2012).
- [32] N. Lindvall, A. Kalabukhov, and A. Yurgens, Cleaning graphene using atomic force microscope, J. Appl. Phys. 111, 064904 (2012).
- [33] Y.-C. Lin, C.-C. Lu, C.-H. Yeh, C. Jin, K. Suenaga, and P.-W. Chiu, Graphene annealing: How clean can it be? Nano Lett. 12, 414 (2012).
- [34] R. Jalilian, L. A. Jauregui, G. Lopez, J. Tian, C. Roecker, M. M. Yazdanpanah, R. W. Cohn, I. Jovanovic, and Y. P. Chen, Scanning gate microscopy on graphene: Charge inhomogeneity and extrinsic doping, Nanotechnology 22, 295705 (2011).
- [35] B. Zhou, Y. Wang, G. B. Osterhoudt, P. Lampen-Kelley, D. Mandrus, R. He, K. S. Burch, and E. A. Henriksen, Possible structural transformation and enhanced magnetic fluctuations in exfoliated α-RuCl₃, J. Phys. Chem. Solids 128, 291 (2018).
- [36] J. A. Elias and E. A. Henriksen, Electronic transport and scattering times in tungsten-decorated graphene, Phys. Rev. B **95**, 075405 (2017).
- [37] J.-H. Chen, C. Jang, S. Xiao, M. Ishigami, and M. S. Fuhrer, Intrinsic and extrinsic performance limits of graphene devices on SiO₂, Nat. Nanotechnol. **3**, 206 (2008).
- [38] Y.-W. Tan, Y. Zhang, K. I. Bolotin, Y. Zhao, S. Adam, E. H. Hwang, S. Das Sarma, H. L. Stormer, and P. Kim, Measurement of Scattering Rate and Minimum Conductivity in Graphene, Phys. Rev. Lett. 99, 246803 (2007).

- [39] S. Adam, E. H. Hwang, V. M. Galitski, and S. Das Sarma, A self-consistent theory for graphene transport, Proc. Natl. Acad. Sci. USA 104, 18392 (2007).
- [40] J.-H. Chen, C. Jang, S. Adam, M. Fuhrer, E. D. Williams, and M. Ishigami, Charged-impurity scattering in graphene, Nat. Phys. 4, 377 (2008).
- [41] A. C. Beer, *Galvanomagnetic Effects in Semiconductors*, Solid State Physics Vol. 42 (Academic, New York, 1963).
- [42] P. D. de Gennes and J. Friedel, Anomalies de resistivite dans certains metaux magnetiques, J. Phys. Chem. Solids 4, 71 (1958).
- [43] M. E. Fisher and J. S. Langer, Resistive Anomalies at Magnetic Critical Points, Phys. Rev. Lett. 20, 665 (1968).
- [44] S. Alexander, J. S. Helman, and I. Balberg, Critical behavior of the electrical resistivity in magnetic systems, Phys. Rev. B 13, 304 (1976).
- [45] O. Rapp, G. Benediktsson, H. U. Astrom, S. Arajs, and K. V. Rao, Electrical resistivity of antiferromagnetic chromium near the Néel temperature, Phys. Rev. B 18, 3665 (1978).
- [46] M. Ausloos and K. Durczewski, Critical behavior of the electrical resistivity in magnetic systems: Comments and theory, Phys. Rev. B 22, 2439 (1980).
- [47] Y.-J. Yu, Y. Zhao, S. Ryu, L. E. Brus, K. S. Kim, and P. Kim, Tuning the graphene work function by electric field effect, Nano Lett. 9, 3430 (2009).
- [48] I. Pollini, Electronic properties of the narrow-band material α -RuCl₃, Phys. Rev. B **53**, 12769 (1996).
- [49] S. Mashhadi, Y. Kim, J. Kim, D. Weber, T. Taniguchi, K. Watanabe, N. Park, B. Lotsch, J. H. Smet, M. Burghard, and K. Kern, Spin-split band hybridization in graphene proximitized with α-RuCl₃ nanosheets, Nano Lett. 19, 4659 (2019).
- [50] R. Hesper, L. H. Tjeng, and G. A. Sawatzky, Strongly reduced band gap in a correlated insulator in close proximity to a metal, Europhys. Lett. **40**, 177 (1997).
- [51] Y. Kubota, H. Tanaka, T. Ono, Y. Narumi, and K. Kindo, Successive magnetic phase transitions in α -RuCl₃: XY-like frustrated magnet on the honeycomb lattice, Phys. Rev. B **91**, 094422 (2015).
- [52] M. Majumder, M. Schmidt, H. Rosner, A. A. Tsirlin, H. Yasuoka, and M. Baenitz, Anisotropic $Ru^{3+}4d^5$ magnetism in the α -RuCl₃ honeycomb system: Susceptibility, specific heat, and zero-field NMR, Phys. Rev. B **91**, 180401(R) (2015).
- [53] M. Ziatdinov, A. Banerjee, A. Maksov, T. Berlijn, W. Zhou, H. B. Cao, J. Q. Yan, C. A. Bridges, D. G. Mandrus, S. E. Nagler, A. P. Baddorf, and S. V. Kalinin, Atomic-scale observation of structural and electronic orders in the layered compound α-RuCl₃, Nat. Commun. 7, 13774 (2016).
- [54] R. Bistritzer and A. H. MacDonald, Moire bands in twisted double-layer graphene, Proc. Natl. Acad. Sci. USA 108, 12233 (2011).